RSC Advances

ROYAL SOCIETY OF CHEMISTRY

www.rsc.org/advances

Structure and Mechanical Properties of Transparent Layered Nanocomposites from Laponite-Hydroxyethyl Cellulose Vacuum-Assisted Self-Assembly

Sukun Zhou, Meng Wang, Jun Yang*, Feng Xu*

MOE Key Laboratory of Wooden Material Science and Application, Beijing Forestry University, Beijing, 100083, China

* Corresponding author, Tel: +86-10-62336387. Fax: +86-10-62336903.

E-mail: yangjun11@bjfu.edu.cn (J. Yang), xfx315@bjfu.edu.cn (F. Xu).

Abstract

Transparent Laponite RD/Hydroxyethyl cellulose (LRD/HEC) nanocomposite films with a full composition range of LRD (0-100 wt%) were fabricated *via* facile vacuum filtration process. The influence of LRD content on the nanostructure and mechanical properties of the nanocomposites was systematically investigated, where exists two critical points at LRD contents of 40 wt% and 70 wt%. In the range of 0-40 wt%, the nanocomposites showed a blurry oriented structure and the mechanical performance of the nanocomposites was improved dramatically with the increase of LRD content. In the range of 40-70 wt%, the nanocomposites showed a clearly oriented lamellar nanostructure with alternating LRD nanoplatelets and HEC layers. The mechanical properties of nanocomposites was further enhanced at a relatively low rate with the increase of LRD content and reached a maximum value at a LRD content of 70 wt%. At this optimum LRD content, the nanocomposites possessed a Young's modulus of 7.09 GPa and a tensile strength of 126.66 MPa, which were 43 times and 5.5 times higher than those of pure HEC films, respectively. Whereas for LRD content was higher than 70%, the lamellar nanostructure was turned to tactoids and deteriorated mechanical properties. It is expected that the results here can offer comprehensive understanding for fabricating bioinspired multilayered nanocomposites.

Keywords: Bioinspired nanocomposites, Laponite, Hydroxyethyl cellulose, Nanostructure, Mechanical properties

1. Introduction

The demand for high-performance, efficient, lightweight materials in transportation, biomedical implant, and defense sector industry is growing at a fast pace. This trend makes a challenge for innovative engineering design to combine the exceptional strength with high toughness. However, the two properties tend to be mutually exclusive, and improving the strength is usually achieved by compromising the toughness, which is not desired for high-performance materials.[1-3] Natural composites provide excellent examples of light-weight, strong, stiff, and tough materials like nacre, crustacean cuticles and bone. Such biocomposites exhibit a brick-and-mortar architecture in which large fractions of hard inorganic nanoplatelets are coated with a thin soft organic layer and ordered in hierarchical arrangement. The hard inorganic nanoplatelets provide strength, while the soft organic layer dissipates viscoplastic deformation energy thus providing a high toughness to the biocomposites.[4, 5]

In the fabrication of bioinspired nanocomposites, biodegradable polymers such as chitosan,[6] carboxymethyl cellulose [7] and polyvinyl alcohol [8, 9] have been widely used as organic polymer matrices. Hydroxyethyl cellulose (HEC) is an amorphous cellulose derivative with high strength and toughness. Due to its renewable, environmentally friendly and nontoxic properties, HEC often used as wound dressing and thickening agent. The high molecular weight and plenty of hydroxyl groups on the surface of HEC promote the formation of hydrogen bonds between HEC and other constituent easily. For example, Sehaqui prepared stretchable HEC-coated cellulose/clay nanocomposites with high strength and toughness, and HEC/clay nanocomposites with high toughness, thermal, and barrier performance. [4, 10-12] Moreover, inorganic nanoplatelets

such as Al_2O_3 platelets,[3] nanotube,[13] clay,[14, 15] graphene[16] and layered double hydroxides (LDHs) [17] have been widely used to fabricate the bioinspired nanocomposites. Laponite a synthetic clay material made from natural minerals and it has 2:1 phyllosilicate structure with an empirical formula: $Na_{0.7}^{+}$ $[(Si_8Mg_{5.5}Li_{0.3})$ O_{20} $(OH)_4]^{0.7}$. It has interesting features such as natural abundance, high aspect ratio and fine established intercalation chemistry.[14] The addition of Laponite in polymers leads to nanocomposites exhibiting enhancements in strength, modulus and thermal properties, while retaining a high degree of optical transparency.[18]

Mimicking the hierarchical structure has been achieved by several strategies， including Layer-by-Layer deposition (LBL),[3, 18-20] vacuum filtration assembly,[21-24] doctor blading technique,[5] air-water interface assembly technique,[3, 17] freeze casting assembly,[25, 26] and evaporation process.[8, 9] LBL has been widely used to assemble oppositely charged inorganic and organic components into thin films with hierarchical structure. Although LBL technique can make a fine control of the layered structure, while it is time-consuming, laborious, and hard to be scaled up.[27] Air-water interface assembly technique is similar to LBL, it is time-consuming but has a fine control of hierarchical structure.[17] Freeze casting is a three-step method where a hierarchical template of the inorganic nanoplatelets is formed by single-track freezing of the suspension, followed by sublimation and template-filling with the organic component.[25] Doctor-blading technique is simple and fast, but it is difficult to control the structure of the composites, then the nanocomposites often have poor mechanical performance.[9] Evaporation process is economical and simple, but it is still time-consuming and has a high requirement for the stability of the dispersion.[8] Compared with the above fabrication methods, the vacuum

filtration assembly is promising as it is energy-efficient, environmentally friendly, economic and is ready for scale-up via continuous processes.[28] Composites of trimethylammonium-modified nanofibrillated cellulose and layered silicates were prepared by vacuum filtration. The composites had an oriented structure and great barrier and mechanical performance.[29] Putz[30] fabricated graphene oxide–polymer nanocomposites by vacuum filtration and the tensile strength was up to 148 MPa. Liu[31] prepared clay-nanocellulose paper by vacuum filtration and the nanopaper showed potential in the application of package industry.

It has been reported that the volume fraction of the inorganic nanoplatelets significantly dominates the performance of nanocomposites.[19] The low-volume addition (1-10%) of nanoplatelets often leads to significant mechanical properties enhancement.[20-22] Theoretically, the mechanical properties can be further enhanced by increasing the volume of nanoplatelets. However, high-volume additions of nanoplatelets often lead to structural inhomogeneities and reduced performance. Therefore, the deficiency in the properties of the nanocomposites is largely related to the difficulty of obtaining well-dispersed large volume fractions of the reinforcing nanoplatelets and a lack of structural control. In the present study, we study the preparation of multilayered Laponite RD (LRD)/ hydroxyethyl cellulose (HEC) nanocomposites *via* vacuum filtration assembly technique. The LRD content in the nanocomposites is tailored between a 0-100 wt% full range, and the effect of LRD content on the structure and mechanical properties of the nancomposites is systematically investigated. It is expected that the results here would shed some insight into developing bioinspired layered nanocomposites for practical applications.

2. Experimental

2.1. Materials

Hydroxyethyl cellulose (HEC) with a viscosity of 4500 ~ 6500 mPa·s (2 wt% in water at 25 °C) was purchased from Sigma Aldrich. Laponite RD (LRD) was purchased from Rockwood and the average diameter and height of the nanoplatelets are about 50 ± 10 nm and 1.5 ± 0.2 nm as described by the manufacturer. Milli-Q water was used for all experiments.

2.2. Preparation of LRD/HEC Nanocomposite Films

A 0.5 wt% LRD dispersion was prepared by dispersing LRD (5 g) in water (1 L) under vigorous stirring followed by removal of unexfoliated LRD by gravitation. After gravitation, the supernatant solution was weighed, dried and reweighed to determine LRD mass concentration. The concentration of the fine LRD suspension was typically 0.45 wt%. HEC (5 g) powder was dissolved in water (1 L) at 80 °C under mild stirring to form an aqueous solution. HEC/LRD nanocomposite films with 10-100 wt% LRD were prepared as follows. A desired amount of the HEC solution was gradually added to the above LRD solution to obtain mixture dispersions with weight ratios of LRD to HEC from 1:9 to 9:1, named as L10/H90, L20/H80, L30/H70, L40/H60, L50/H50, L60/H40, L70/H30, L80/H20, L90/H10, respectively.

The mixed dispersion was continually stirred for 4 h and then was further dispersed for 30 min by ultrasonication (Ningbo Xinzhi JY99-IIDN Probe 25 mm) at 500W to maximize polymer adsorption and ensure fine dispersion of the stabilized LRD nanoplatelets. The HEC molecules are very easily coated onto the exfoliated LRD nanoplatelets to yield the HEC-coated LRD

building blocks by strong electrostatic and hydrogen-bonding interactions. When the LRD/HEC suspension is first filtered through a filtration paper, only little of the HEC chains initially pass through; however, this process is quickly hindered by the deposition of the HEC-coated LRD building blocks, which can be aligned to a layered microstructure by vacuum filtration induced self-assembly because of the role that the orientation of the nanoplatelets and linking of the HEC play. The filtration time ranged from 20 to 60 min, depending on the thickness of the final films and the content of LRD. After filtration, the wet films were dried at room temperature for 48 h and then the nanocomposite films were obtained by dissolving the cellulose acetate filtration paper in acetone. As reference, pure HEC films were prepared by casting a 0.5 wt% aqueous solution of HEC into a petri dish and allowing water to evaporate at room temperature for 48 h.

2.3. Characterization

Atomic force microscope (AFM) images were acquired using a SPM-9500J3 AFM. A freshly cleaved mica slide was used as the substrate for the AFM measurement and one drop of the solution of sample was dropped on the substrate and dried naturally for the AFM characterization. Transmission electron microscopy (TEM) was performed on a JEOL JEM-3200FSC Cryo-TEM, operating at liquid nitrogen temperature. The images were taken in bright field mode and using zero loss energy filtering with the slit of 20 eV. Tensile fractured specimens were used for SEM observation and these were first dried in a desiccator overnight. Then the cross sections of the nanocomposite films were observed with a JEOL JSM-7500 scanning electron microscope after sputter-coating a thin gold layer. XRD patterns of nanocomposites films and pure LRD powder

were recorded by a D8-Advance X-ray Diffraction Analyzer at room temperature. The Cu Kα radiation source was operated with a tension of 40 kV and a current of 35 mA (λ =1.5406Å). Patterns were recorded by monitoring diffractions from 3° to 25°. An increment step of 0.05° and a rate of 1 step per 5 seconds were used. Fourier transform infrared spectroscopy (FTIR) was performed on an infrared spectrophotometer (Nicolet iN10-MX, ThermoScientific). The light transmittance of the films was measured by a UV2300 spectroscopy.

Static tensile mechanical properties of nanocomposite films and reference HEC films were performed using a Zwick-Z005 Tester with a load cell of 500 N at room temperature. The rectangular specimen strips were about 40 mm in length, and 5 mm in width. The distance between the clamps was 15 mm and the load speed was 0.1 mm min^{-1}, five specimens were tested for each sample. Young's modulus was determined from the slope of initial low strain region. Toughness was calculated as the area under the stress-strain curves. Thermogravimetric Analysis (TGA) was conducted to evaluate the thermal properties of nanocomposite films and this was performed on a Shimadzu DTG-60 thermal analyser from 40 to 800 °C with a heating rate of 20 °C min^{-1} under nitrogen atmosphere with a flow rate of 50 mL min^{-1}. The density of the nanocomposite films (ρ) was determined from their volume and weight, the volume is taken as the arithmetic product of the thickness and the surface area of the films. The thickness was measured using a film gauge with an accuracy of 1 μm. Then the porosity of the nanocomposites was calculated from their density by taking 625 and 1000 kg m^{-3} (provided by the manufacturer) as density for HEC and LRD, respectively, using eq.1.

$$\text{porosity} = 1 - \frac{\rho}{\left(\frac{w_{LRD}}{\rho_{LRD}} + \frac{w_{HEC}}{\rho_{HEC}}\right)^{-1}} \quad (1)$$

Volume fraction of LRD was calculated using eq. 2.

$$V_{LRD} = \frac{\rho_{HEC} w_{LRD}}{\rho_{LRD} w_{HEC} + \rho_{HEC} w_{LRD}} \quad (2)$$

V and *W* refer to LRD volume and weight fraction, respectively.

3. Results and discussion

3.1. Structure of the nanocomposite films

The LRD nanoplatelets were exfoliated by mechanical stirring and the unexfoliated LRD was removed by gravitation. Fig. 1 illustrates that the aqueous suspension of LRD is transparent and stable, without virtually no precipitation of LRD aggregates even after a week. The HEC-coated LRD hybrid building blocks were prepared by mixing an aqueous suspension of exfoliated LRD nanoplatelets and an aqueous suspension of HEC. The resulting mixture suspension was stirred for 4 h and then was further dispersed for 30 min by ultrasonication to allow the HEC molecules to fully adsorb onto the surface of the LRD nanoplatelets. Fig. 1 shows that the hazy LRD/HEC mixed suspension is very stable, even after a week.

The LRD colloidal suspension and LRD/HEC mixed dispersions was examined by AFM and TEM, as shown in Fig. 2. The individual nanoplatelet with average diameter about 60 nm is observed in Fig. 2(a), indicating the complete exfoliation of LRD. According to Fig. 2(b), the HEC polymer chains are adsorbed onto the LRD nanaplatelets surface and the HEC-coated LRD nanoplatelets tend to form a ‘shell’ on the substrate due to the adsorption of HEC. Further

observation at higher magnifications (Fig. 2(b), inset) indicates that LRD nanoplatelets are embedded in the matrix homogeneously with the surrounding HEC. Since there are a large amount of hydroxyl groups on the surface of HEC and numerous oxygen functional groups on the basal planes and edges of the LRD nanoplatelets,[32] it leads to the formation of rich hydrogen bonding between HEC and LRD. Moreover, the vacuum filtration process would increase the extent of hydrogen bonding between HEC and LRD and form a strong interfacial attachment for stress transfer.[33, 34] As hydrogen bonding only occur over a short distance (<3 Å[35]), specific orientation of the HEC-coated LRD building blocks is required for their formation and the vacuum filtration process could promote the oriented alignment of the HEC-coated LRD building blocks.

The optical photographs and light transmittance of the nanocomposite films are presented in Fig. 3, and the results show that the films are apparent, flat and smooth, similarly to the films prepared by other system.[10, 21] Pure HEC film has light transmittance of 92% at 600 nm and the LRD/HEC nanocomposite films show high light transmittance of 60%-85% as the LRD content less than 70 wt % (Fig. 3(b)). The high light transmittances of the LRD/HEC nanocomposite films reveal that LRD nanoplatelets, which have much smaller dimensions than optical wavelengths, are mostly dispersed as individual nanoplatelet in the HEC matrix without significant aggregation, although small nanoplatelet agglomerates may also be present. However, as LRD content exceeds 70 wt%, the films exhibit notably lower transmittances, probably due to the LRD aggregation in the matrix.

Fig. 4 shows the morphology of cross-section of the fractured samples. For low LRD content

(Fig. 4(a) (b)), the cross-section of the nanocomposites does not clearly show the layered struction, because the HEC is wrapped in the LRD nanoplatelets. In contrast, when the LRD content surpasses 40 wt% (Fig. 4(c) (d)), a desired hierarchical structure throughout the thickness of the film like that of nacre appears where each layer is parallel to the film surface and interpenetrates into neighboring layers. Such laminated structure also appeared in other biomimetic inorganic-organic nanocomposites prepared by other fabrication system.[36, 37] When the LRD content surpasses 70 wt% (Fig. 4(e) (f)), HEC is insufficient to cover all the LRD nanoplatelets and the LRD nanoplatelets aggregate to tactoids.

Diffractograms and *d*-space values for pure LRD and the nanocomposite films are shown in Fig. 5. The pure LRD has a reflection peak at 9.3° corresponding to a d_{001} lattice spacing of 0.98 nm. The addition of HEC shifts the peaks to a lower angle indicating the intercalation of HEC between LRD galleries. The *d*-space values for HEC/LRD nanocomposites with 10-30 wt% HEC are about 1.06-1.22 nm which means the galleries distance nearly unchanged compared with that of the pure LRD, suggesting that most HEC molecules only adsorb on the edges of LRD nanoplatelets by hydrogen bonding. Moreover, the nanocomposites with 10-30 wt% HEC exhibit a broad peak and partly overlap the peak of pure LRD, indicating that partial LRD nanoplatelets are re-aggregated and form tactoids, probably because the amount of HEC is too small to cover all the LRD nanoplatelets. As HEC contents range from 40 wt% to 60 wt%, the *d*-space values increase to 1.43-1.81 nm which is ascribed to the intercalation of HEC molecules in galleries between individual LRD nanoplatelets. The *d*-space values increase with increasing HEC content, suggesting the desired control of the layered structure of the nanocomposites. No apparent peaks

is detected as HEC content surpasses 60 wt% revealing the complete exfoliation of LRD.

3.2. Interactions between HEC and LRD

FTIR spectroscopy was used to examine the interactions between HEC and LRD. Fig. 6 shows the FTIR spectra of HEC, LRD and nanocomposite films with different LRD content. The frequency of vibrational bands at 3410 cm^{-1} and 3480 cm^{-1} correspond to hydroxyl groups in LRD and HEC, respectively. For L40/H60, L50/H50 and L70/H30 nanocomposite films, the intensity of hydroxyl groups is weakened and shifted toward lower frequency value (3380 cm^{-1}) compared with that of pure HEC. This is ascribed to the adsorption of HEC on the LRD nanoplatelets and the formation of hydrogen bonding between the LRD and HEC, which decreases the extent of intermolecular hydrogen bonding in HEC. This result is in agreement with the TEM micrograph that the HEC is adsorbed on the LRD nanoplatelets. Besides, the frequency of vibrational bonds at 1050 cm^{-1} and 995 cm^{-1} are assigned to C-O-C bonds in HEC and Si-O bonds in LRD, respectively. For nanocomposite films, the addition of LRD shifts the frequency of C-O-C bonds toward lower frequency value and this indicates the incorporation of HEC and LRD. Nevertheless, no peaks at 839 cm^{-1} are observed suggesting the absence of Al-O-C bonds, and this may account for the lower mechanical properties of our nanocomposites compared to other clay/PVA nanocomposites.[8, 9]

3.3. Mechanical properties

The mechanical properties of the nanocomposite films were measured by tensile measurements. Fig. 7 shows the stress-strain curves of the nanocomposites, and the tensile properties at different

LRD content are summarized in Table 1. Pure HEC film has an initial elastic deformation (ε < 6%) followed by a large plastic deformation (6% < ε < 115%), with a tensile strength of 23.62 MPa. The Young's modulus, yield strength and strain at fracture are about 0.16 GPa, 8 MPa, and 115%, respectively. For nanocomposites with 10 wt% - 30 wt% LRD content (Figure 7(a)), the stress-strain curves exhibit an obvious yield point, and the yield strength, Young's modulus and ultimate strength are enhanced remarkably with the increasing of LRD content. For nanocomposites with 40 wt% - 70 wt% LRD content (Fig. 7(b)), the yield point disappears and the Young's modulus and ultimate strength are further improved along with a dramatic decrease in strain at fracture values. The Young's modulus and ultimate tensile strength of the nanocomposite reach maximum values at a LRD content of 70 wt%. At this optimal LRD content, the nanocomposites possess a Young's modulus of 7.09 GPa and a ultimate tensile strength of 126.66 MPa, which are 43 times and 5.5 times higher than those of pure HEC films, respectively. However, the Young's modulus and strength of the nanocomposite are significantly reduced as the LRD content is higher than 70 wt %. There is no data about pure LRD film and L10/H90 nanocomposite films because they are too brittle for measurement.

Fig. 8 (a-c) show the Young's modulus, ultimate tensile strength and strain at fracture values of the LRD/HEC nanocomposites at different LRD content. The effect of the LRD content on the mechanical properties of nanocomposite films can be quantified by the rate of increase of Young's modulus (E) and strength (σ) with the weight fraction of LRD (φ). According to evolvement of the Young's modulus, strength and strain at fracture, the LRD weight fraction could be divided into three regions: 0-40 wt%, 40-70 wt%, and 70-100 wt%. For the region of

0-40 wt%, the Young's modulus and strength of nanocomposite films increase sharply and achieve a much larger extent compared with conventionally polymer systems enhanced by micron-sized fillers.[38] The rate of increase of the Young's modulus and strength with φ, $dE/d\varphi$ and $d\sigma/d\varphi$ reach about 11.25 GPa and 265 MPa, respectively. In the region of 40-70 wt%, the Young's modulus and strength further increase as LRD content increases. However, compared with the first region, the rate of increase of the Young's modulus and strength is lower. $dE/d\varphi$ and $d\sigma/d\varphi$ are about 8.33 GPa and 66.67 MPa, respectively. Whereas in the region of 70-100 wt%, the Young's modulus and strength of the nanocomposite films turn to reduce with the increase of the LRD content. For all the three regions, the strain at fracture values decrease dramatically with the increase of LRD content.

Fig. 8 (d) summarizes the mechanical properties of our layered LRD/HEC nanocomposites and other reported layered clay/polymer nanocomposites prepared by vacuum filtration without crosslinks. The Young's modulus and strength data of the nanocomposite containing 70 wt% LRD content are comparable to date for cellulose nanofibers/MTM nanocomposite,[21] chitosan/MTM hybrids,[22] CMC/MTM nanocomposits [39] and PVA/Laponite multilayer films,[37] while they are lower than cellulose nanofibers/PVA/MTM films,[8] PVA/MTM hybrids [9] and PVA/LDH nanocomposites.[27] Nevertheless, our strain at fracture value is higher than any other multilayered nanocomposites with similar inorganic content (usually below 2%). Even with a tough cellulose nanofiber matrix, the nanocomposites strain at fracture value is still around 2%.[39] The high ductility could be explained by the porosity in the nanocomposite films. For example, the films with 70 wt% LRD content have a density of 664 kg m^{-3}, and this indicates about 18%

porosity in the films as non-porous films would have a density of 810 kg m^{-3} (eq.1-2). The density and porosity of the nanocomposites are present in Table S1 in the supporting information. The pores present in the interface of the HEC-rich and LRD-rich regions are beneficial for a higher ductility of the films as they offer large room for HEC chains rearrangements.[40] Thus, our nanocomposite films possess both exceptional ductility and toughness (the area under stress-strain curve) at a relatively high clay content.

3.4. Thermogravimetric Analysis

Thermal degradation of the nanocomposites has been evaluated by thermogravimetric analysis (TGA). The typical thermograms for pure HEC and LRD/HEC nanocomposites are presented in Fig. 9. Pure HEC film has an onset degradation temperature of 250 °C and the degradation rate is very fast. With the addition of LRD, the onset degradation temperature for the nanocomposites is delayed to 300 °C and the degradation rate is dramatically decreased. Enhancement of thermal degradation behavior of the nanocomposite films with respect to the pure polymer also has been reported in other articles.[7, 31] The main reason for the enhanced thermal properties is that the LRD nanoplatelets form continuous protective solid layers, and the adsorbed HEC polymer chains on LRD nanoplatelets surface leads to a dense structure of the nanocomposite films, thus the oxygen diffusion rate is reduced and the oxidation kinetics becomes lower. Moreover, silicate layer char and fusion formation of HEC also contribute to the better thermal properties.

3.5. Networks of LRD/HEC nanocomposites

Taken together, a schematic illustration of the proposed nanocomposites network structure is presented in Scheme 1. The nanocomposites with LRD weight fraction range of 0 wt% and 40 wt% have a blurry oriented structure (Scheme 1 (a)) because of the excess HEC. In this range, increasing the content of LRD nanoplatelets within the matrix leads to a significant increase of Young's modulus and strength along with a dramatic decrease in strain at fracture value. The high increase rate of Young's modulus and strength ($dE/d\varphi$ = 11.25 GPa, $d\sigma/d\varphi$ = 265 MPa) could be ascribed to the LRD-induced HEC interfacial phase, which has a higher modulus and strength than that of bulk HEC phase, and the fraction of the LRD-induced HEC interfacial phase increases with increasing LRD content [41]. The nancomposites with LRD weight fraction between 40 wt% and 70 wt% have a multilayered structure (Scheme 1 (b)). HEC chains are completely constrained by LRD nanoplatelets and this leads to the lower increase rate of Young's modulus and strength ($dE/d\varphi$ = 8.33 GPa, $d\sigma/d\varphi$ = 66.67 MPa). When the LRD content surpasses the critical nanoplatelet fraction (40 wt%), most of the HEC chains in the nanocomposites are stiffened by the LRD nanoplatelets. It can be considered that as the LRD content further increases, the additional exfoliated LRD nanoplatelets are induced into the HEC region which has been affected by other LRD nanoplatelets. In other words, increasing LRD content does not change the fraction of the interphase polymer.[9]

With further increasing of LRD content, the multilayered structure of nanocomposites with LRD weight fraction between 70 wt% and 100 wt% is transformed to aggregation (Scheme 1 (c)). The total amount of HEC is insufficient to completely intercalate all LRD nanoplatelets and HEC is not present as a continuous layer. In this case, the lack of HEC leads the LRD nanoplatelets to

form aggregation, which inevitably deteriorate the mechanical properties of the nanocomposites. The analysis above demonstrates that the appropriate content of the two constituents and the interfacial bonding between the two constituents play important role on the load transfer efficiency from ductile polymer to the hard inorganic phase. High volume of inorganic nanoplatelets in the nanocomposites would damage the layered structure and reduce the mechanical properties of the nanocomposites. Therefore, it is still a challenge to control the structure of nanocomposites with high volume of inorganic nanoplatelets and systematically understand the mechanical interactions of the two constituents at the nanoscale.

4. Conclusion

Vacuum filtration technique was used to assemble LRD nanoplatelets and HEC into films with a full composition range of LRD (0-100 wt%). Low-volume additions (0-40 wt%) of LRD generate a blurry oriented structure and significant improvement of mechanical properties, due to the unique interphase reinforcement mechanism. For high-volume additions (40-70 wt%), the random structure is turned into a multilayered structure, and the mechanical properties is further increased at a relatively slow rate. At a critical LRD nanoplatelets content of 70 wt%, the Young's modulus and strength reach 7.09 GPa, 126.66 MPa, respectively, which are 43 times and 5.5 times those of pure HEC films. The strain at fracture value is 3.16%, which is higher than other nacre-like layered nanocomposites with similar inorganic content. For the LRD nanoplatelets exceeds 70 wt%, the LRD nanoplatelets aggregate and the aggregation would reduce the mechanical performance of the nanocomposites. The analysis of the relationship between

inorganic content with the structure and mechanical performance of the nanocomposites would deepen the understanding of the structure of bioinspired layered nanocomposites. Furthermore, the scalable and green preparation route, combined with high mechanical, thermal, and optical performance of the prepared nanocomposite films may promote their practical applications in packaging, transportation, construction, and insulation industry.

Acknowledgements

This work was financially supported by China National Funds for Distinguished Young Scientists (31225005), Fundamental Research Funds for the Central Universities (TD2011-10), the Doctoral Program of Higher Education of China (20120014120006), and Chinese Ministry of Education (113014A).

References

1. G. Mayer, *Science*, 2005, **310**, 1144-1147.
2. M. A. Meyers, P.Y. Chen, A. Y.M. Lin and Y. Seki, *Prog. Mater. Sci.*, 2008, **53**, 1-206.
3. L. J. Bonderer, A. R. Studart and L. J. Gauckler, *Science*, 2008, **319**, 1069-1073.
4. H. Sehaqui, J. Kochumalayil, A. Liu, T. Zimmermann and L. A. Berglund, *ACS Appl. Mater. Inter.*, 2013, **5**, 7613-7620.
5. P. Das, S. Schipmann, J.M. Malho, B. Zhu, U. Klemradt and A. Walther, *ACS Appl. Mater. Inter.*, 2013, **5**, 3738-3747.
6. E. Günister, D. Pestreli, C. H. Ünlü, O. Atıcı and N. Güngör, *Carbohyd. Polym.*, 2007, **67**,

358-365.

7. E. Burgaz, *Polymer*, 2011, **52**, 5118-5126.

8. J. Wang, Q. Cheng, L. Lin and L. Jiang, *ACS Nano*, 2014, **8**, 2739-2745.

9. J. Wang, Q. Cheng, L. Lin, L. Chen and L. Jiang, *Nanoscale*, 2013, **5**, 6356-6362.

10. H. Sehaqui, A. Liu, Q. Zhou and L. A. Berglund, *Biomacromolecules*, 2010, **11**, 2195-2198.

11. H. Sehaqui, S. Morimune, T. Nishino and L. A. Berglund, *Biomacromolecules*, 2012, **13**, 3661-3667.

12. H. Sehaqui, Q. Zhou and L. A. Berglund, *Soft Matter*, 2011, **7**, 7342-7350.

13. B. S. Shim, J. Zhu, E. Jan, K. Critchley, S. Ho, P. Podsiadlo, K. Sun and N. A. Kotov, *ACS Nano*, 2009, **3**, 1711-1722.

14. L. Liu, Z. Qi and X. Zhu, *J. Appl. Polym. Sci.*, 1999, **71**, 1133-1138.

15. S. Huang, S. L. Phua, W. S. Liu, G. Q. Ding and X. H. Lu, *RSC Advances*, 2014, **4**, 1425-1431.

16. Y. Wang, J. R. Yu, L. Chen, Z. M. Hu, Z. X. Shi and J. Zhu, *RSC Advances*, 2013, **3**, 20353-20362.

17. H.B. Yao, H.Y. Fang, Z.H. Tan, L.H. Wu and S.H. Yu, *Angew. Chem. Int. Edit.*, 2010, **49**, 2140-2145.

18. E. R. Kleinfeld and G. S. Ferguson, *Science*, 1994, **265**, 370-373.

19. A. J. Svagan, A. Akesson, M. Cardenas, S. Bulut, J. C. Knudsen, J. Risbo and D. Plackett, *Biomacromolecules*, 2012, **13**, 397-405.

20. G. Decher, *Science*, 1997, **277**, 1232-1237.

21. A. Liu, A. Walther, O. Ikkala, L. Belova and L. A. Berglund, *Biomacromolecules*, 2011, **12**, 633-641.

22. H.B. Yao, Z.H. Tan, H.Y. Fang and S.H. Yu, *Angew. Chem. Int. Edit.*, 2010, **49**, 10127-10131.

23. L. Martikainen, A. Walther, J. Seitsonen, L. Berglund and O. Ikkala, *Biomacromolecules*, 2013, **14**, 2531-2535.

24. A. Walther, I. Bjurhager, J.M. Malho, J. Ruokolainen, L. Berglund and O. Ikkala, *Angew. Chem. Int. Edit.*, 2010, **49**, 6448-6453.

25. S. Deville, E. Saiz, R. K. Nalla and A. P. Tomsia, *Science*, 2006, **311**, 515-518.

26. E. Munch, M. E. Launey, D. H. Alsem, E. Saiz, A. P. Tomsia and R. O. Ritchie, *Science*, 2008, **322**, 1516-1520.

27. P. Podsiadlo, A. K. Kaushik, E. M. Arruda, A. M. Waas, B. S. Shim, J. D. Xu, H. Nandivada, B. G. Pumplin, J. Lahann, A. Ramamoorthy and N. A. Kotov, *Science*, 2007, **318**, 80-83.

28. A. Walther, I. Bjurhager, J. M. Malho, J. Pere, J. Ruokolainen, L. A. Berglund and O. Ikkala, *Nano Lett.*, 2010, **10**, 2742-2748.

29. T. T. Ho, T. Zimmermann, S. Ohr and W. R. Caseri, *ACS Appl. Mater. Inter.*, 2012, **4**, 4832-4840.

30. K. W. Putz, O. C. Compton, M. J. Palmeri, S. T. Nguyen and L. C. Brinson, *Advanced Functional Materials*, 2010, **20**, 3322-3329.

31. A. Liu and L. A. Berglund, *Carbohyd. Polym.*, 2012, **87**, 53-60.

32. Q. Cheng, L. Jiang and Z. Tang, *Accounts Chem. Res.*, 2014, **47**, 1256-1266.

33. Y.J. Lee, S.W. Kuo, W.J. Huang, H.Y. Lee and F.C. Chang, *J. Polym. Sci. Pol. Phys.*, 2004, **42**, 1127-1136.

34. S.W. Kuo and F.C. Chang, *Prog. Polym. Sci.*, 2011, **36**, 1649-1696.

35. C. Schlenk and H. Frey, *Monatsh. Chem.*, 1999, **130**, 3-14.

36. P. Podsiadlo, S. Paternel, J. M. Rouillard, Z. F. Zhang, J. Lee, J. W. Lee, L. Gulari and N. A. Kotov, *Langmuir*, 2005, **21**, 11915-11921.

37. T. U. Patro and H. D. Wagner, *Nanotechnology*, 2011, **22**, 455706.

38. T. D. Fornes and D. R. Paul, *Polymer*, 2003, **44**, 4993-5013.

39. A. Liu and L. A. Berglund, *Eur. Polym. J.*, 2013, **49**, 940-949.

40. J. Wu and M. M. Lerner, *Chem. Mater.*, 1993, **5**, 835-838.

41. G. E. Padawer and N. Beecher, *Polym. Eng. Sci.*, 1970, **10**, 185-192.

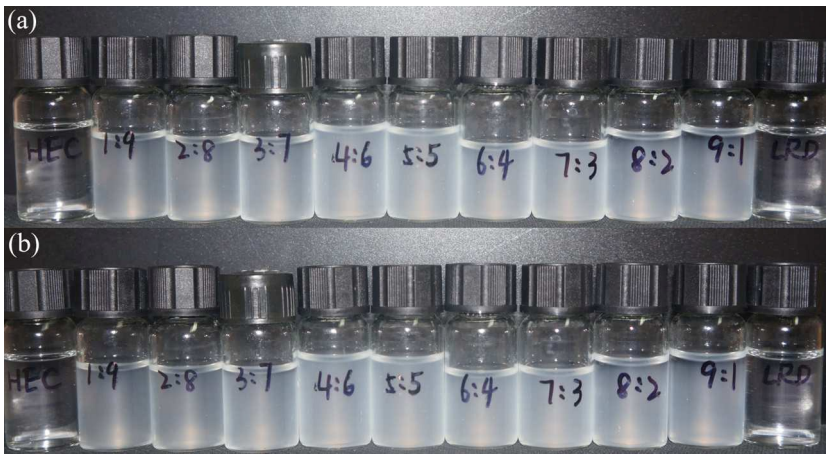

Fig. 1 (a) Photograph of HEC, LRD and LRD/HEC suspensions (b) after standing for a week.

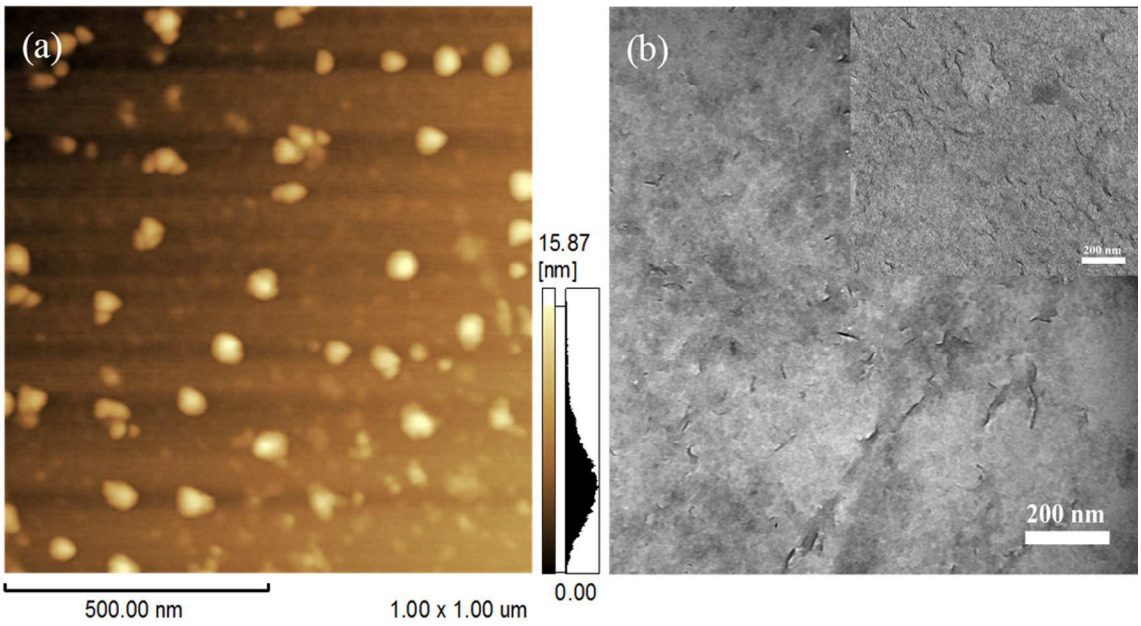

Fig. 2 (a) Atomic force microscopy image of LRD nanoplatelets deposited on mica. (b) Transmission electron microscopy image of HEC-coated LRD nanoplatelets, suggesting the dramatic exfoliation and homogeneous dispersion of LRD in the matrix.

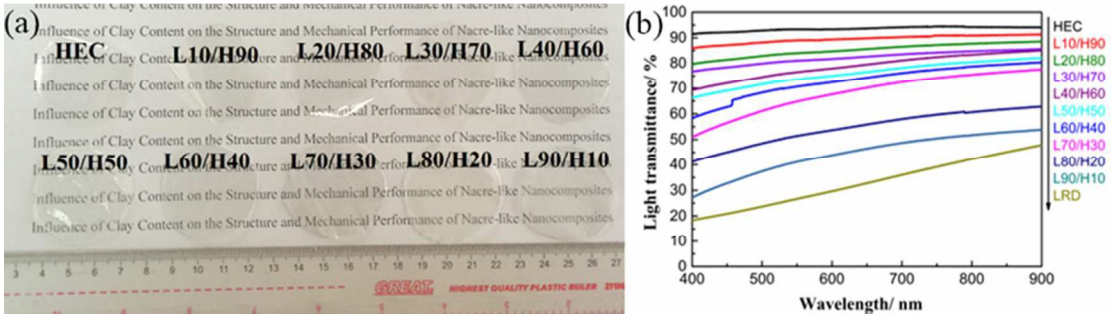

Fig. 3 (a) Photograph and (b) light transmittances of LRD/HEC nanocomposite films with different LRD content. The thickness of the films are about 20-30 μm.

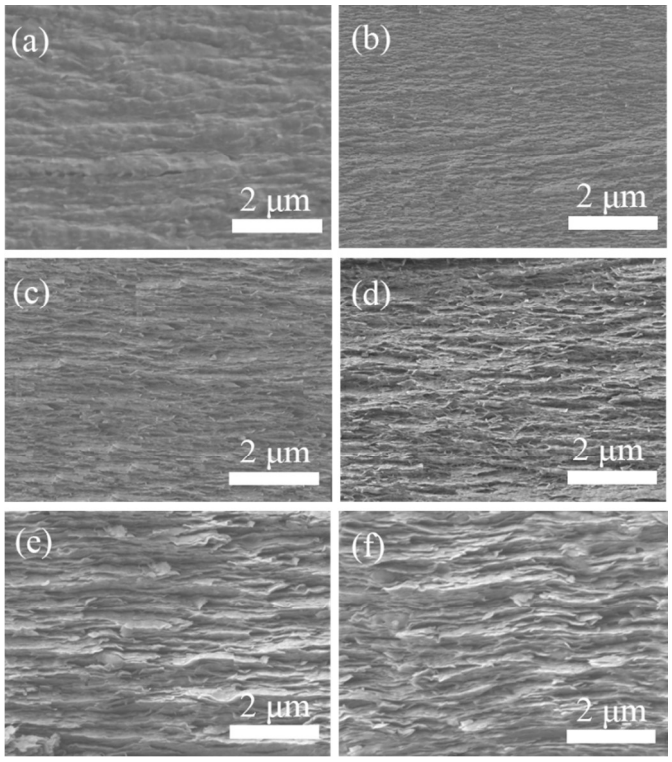

Fig. 4 SEM images of the cross-section LRD/HEC nanocomposite films: (a) L10/H90 (b) L30/H70 (c) L50/H50 (d) L70/H30 (e) L80/H20 (f) L90/H10.

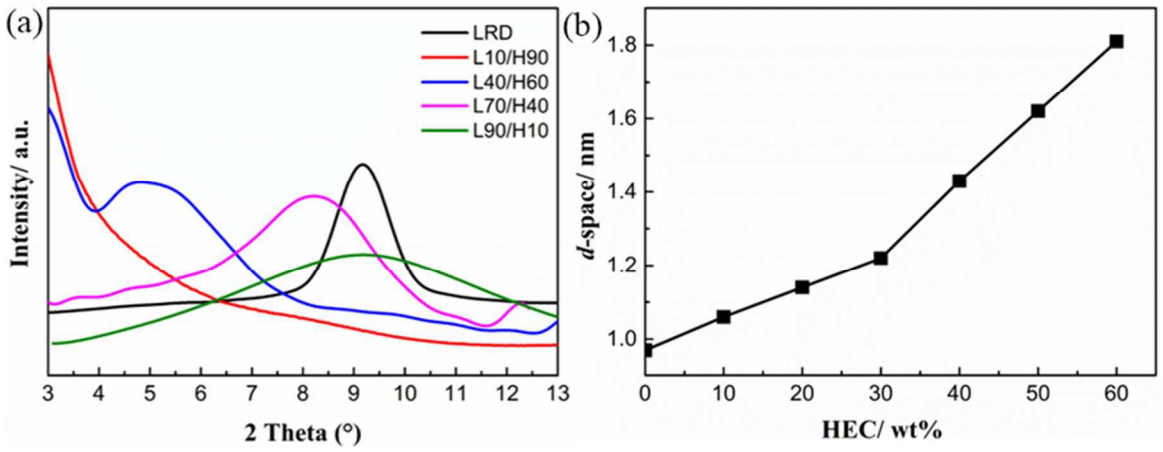

Fig. 5 (a) X-ray diffractograms for pure LRD and LRD/HEC films. (b) *d*-space values for LRD/HEC films as a function of HEC content.

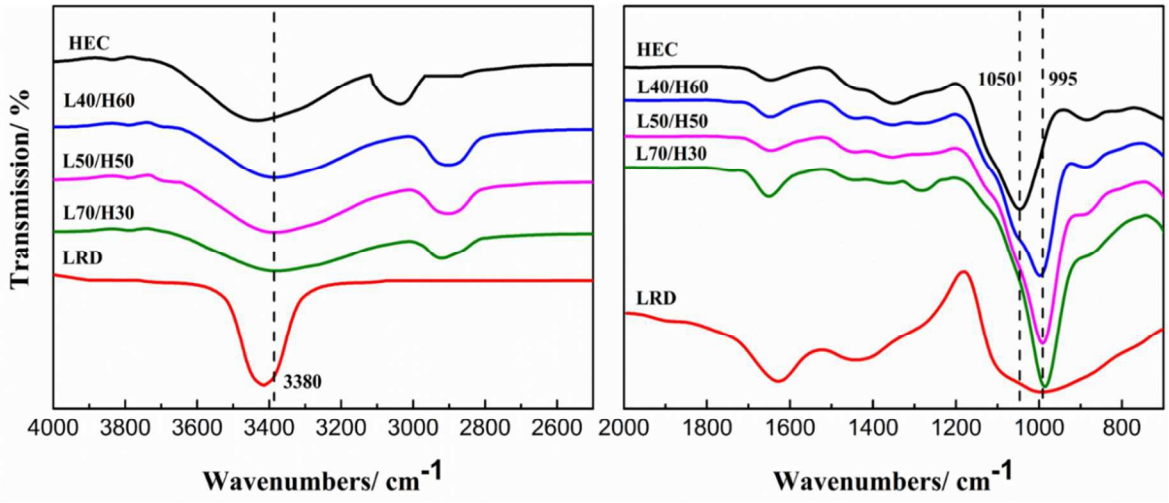

Fig. 6 FTIR spectra ranging from 4000 to 2500 cm^{-1} (a) and from 2000 to 700 cm^{-1} (b) for LRD, HEC and LRD/HEC films.

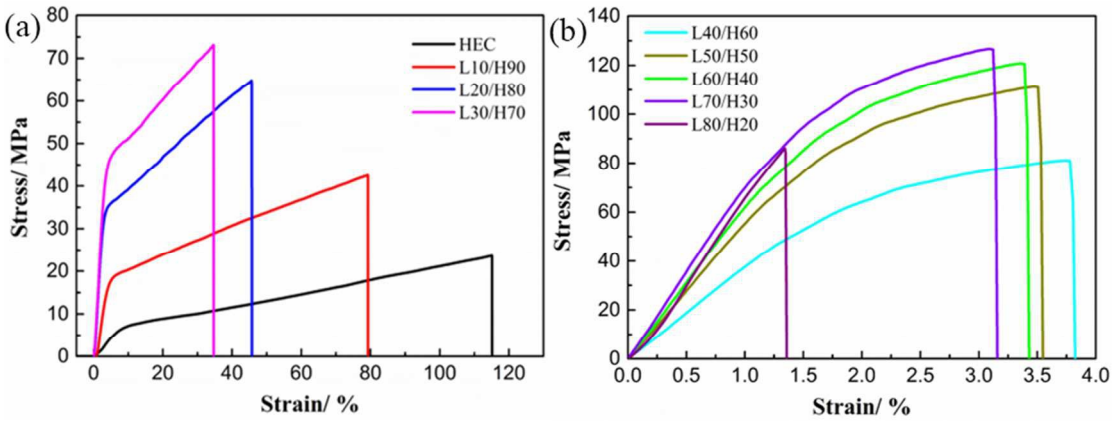

Fig. 7 Stress-strain curves of LRD/HEC nanocomposites with different weigh fraction of LRD. (a) 0 wt%-30 wt%. (b) 40 wt%-80 wt%.

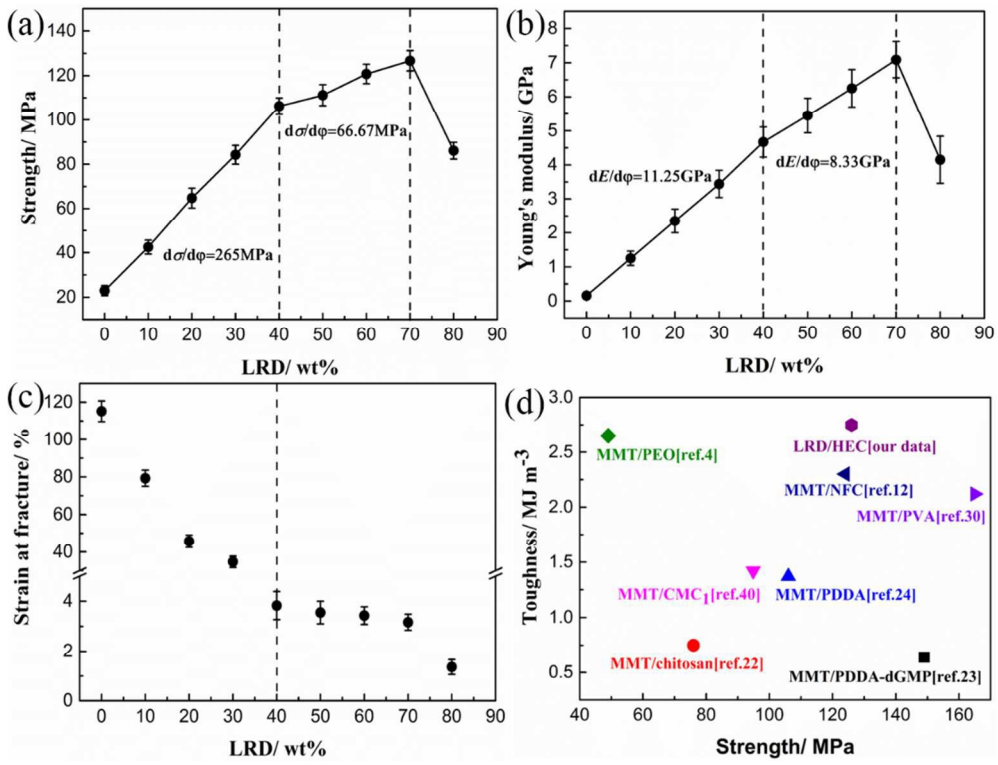

471

472 **Fig. 8** The effect of LRD content on (a) Young's modulus, (b) strength, and (c) strain at fracture.

473 (d) Toughness *vs.* strength of our LRD/HEC nanocomposites compared with other layered

474 clay/polymer nanocomposites.

475

476

477

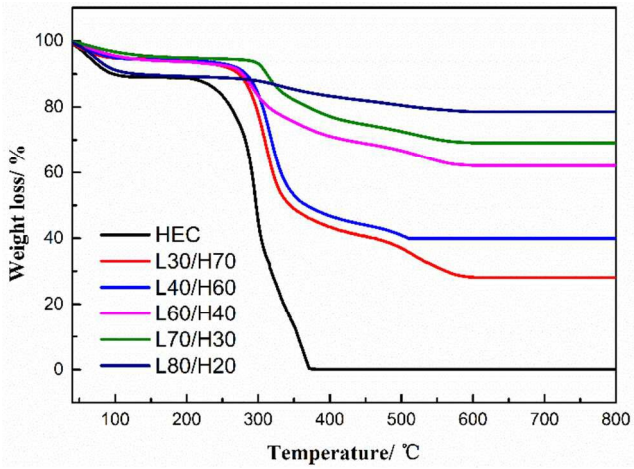

Fig. 9 TGA curves for LRD/HEC nanocomposite films with different LRD contents.

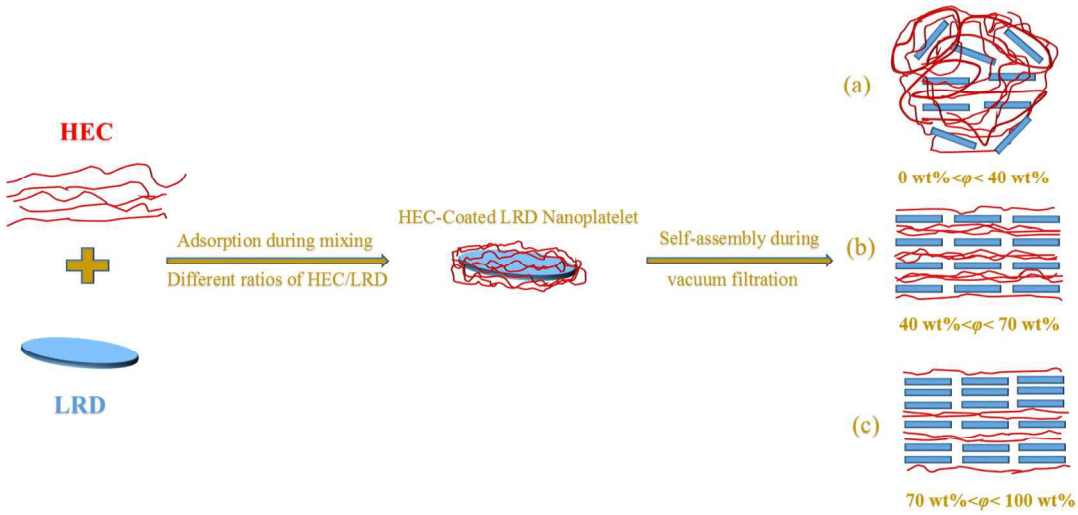

Scheme 1 Proposed structural models of LRD/HEC nanocomposites prepared by vacuum filtration process. (a) Nanocomposites with LRD weight fraction between 0-40 wt%. (b) Nanocomposites with LRD weight fraction between 40-70 wt%. (c) Nanocomposites with LRD weight fraction between 70-100 wt%.

488 **Table 1**

489 LRD content and the tensile mechanical properties of LRD/HEC naocomposites.

Sample	W_{HEC}/W_{LRD}	V_{HEC}/V_{LRD}	LRD content by TGA (wt%)	Modulus (GPa)	Strength (MPa)	Strain at fracture (%)
HEC	100/0	100/0	0	0.16 ± 0.04	22.98 ± 2.25	115.18 ± 5.50
L10/H90	90/10	93/7	11.2	1.25 ± 0.21	42.52 ± 3.14	79.28 ± 4.31
L20/H80	80/20	86/14	20.5	2.35 ± 0.35	64.75 ± 4.51	45.72 ± 3.35
L30/H70	70/30	79/21	36.3	3.44 ± 0.40	84.23 ± 4.25	34.70 ± 3.08
L40/H60	60/40	70/30	41.5	4.67 ± 0.44	106.21 ± 3.74	3.83 ± 0.56
L50/H50	50/50	61/39	51.9	5.45 ± 0.51	111.18 ± 4.73	3.55 ± 0.45
L60/H40	40/60	51/49	64.2	6.25 ± 0.55	120.74 ± 4.39	3.43 ± 0.35
L70/H30	30/70	40/60	71.3	7.09 ± 0.53	126.66 ± 4.55	3.16 ± 0.32
L80/H20	20/80	29/71	81.2	4.15 ± 0.69	86.08 ± 3.78	1.36 ± 0.29
L90/H10	10/90	15/85	86.3	-	-	-
LRD	0/100	0/100	-	-	-	-

490 *W* and *V* refer to weight and volume fraction.